# A 2-D CORRELATION TO EVALUATE FUEL-CLADDING GAP THERMAL CONDUCTANCE IN MIXED OXIDE FUEL ELEMENTS FOR SODIUM-COOLED FAST REACTORS

Lavarenne, J.[a]; Bubelis, E.[b]; Davies, U.[c]; Gianfelici, S.[b]; Gicquel, S.[d]; Krepel, J.[e]; Lainet, M.[f]; Lindley, B.[a]; Mikityuk, K.[e]; Murphy, C.[a]; Perrin, B. [g]; Pfrang, W.[b]; Ponomarev, A.[e]; Schubert, A.[h]; Shwageraus, E.[c]; Van Uffelen, P..

*[a] Wood, United Kingdom; [b]KIT, Germany; [c]University of Cambridge, United Kingdom; [d] EDF, France; [e] PSI, Switzerland; [f] CEA, France; [g] Framatome, France; [h] JRC, Germany;*

*The paper defines a parameterization for the fuel-cladding gap thermal conductance in a Sodium Cooled Fast Reactor. This collaboration took place within the EU-funded ESFR-SMART project.*
*This requires use of predictive codes that have been validated where possible against experimental data. This study relied on 7 fuel performance codes thus providing confidence in the recommended correlation.*

*A single pin model for both the inner and outer fuel was built. The fuel was burned for 2100 Effective Full Power Days, with the axial power distribution varying over time.*

*This paper presents a comparison between the codes' results and a 2-D correlation for the heat conductance with respect to fuel burn-up and fuel rating. The fuel is broken down into nodes with specific fuel rating and burn-up, leading to the gap conductance expressed as a function of nodal fuel rating and burn-up. Data was then compiled for all the nodes, for both fissile and fertile regions, for both inner and outer fuel for all 7 codes. A 2D fit was applied to the data thus obtained.*

*The results obtained show a general increase of heat conductance with fuel rating and burn-up, from 0.22 at 0 burn-up and 10* $kW.m^{-1}$ *to 0.45* $W.cm^{-2}.K^{-1}$ *at 0 burn-up and 50* $kW.m^{-1}$ *and to 1.00* $W.cm^{-2}.K^{-1}$ *at 150* $GWd.t^{-1}$ *and 50* $kW.m^{-1}$*. Some spread between codes has been noted and appears to be consistent with the spread published earlier by several code developers.*

*Sensitivity to various modelling assumptions is under investigation. This is aided by the use of numerous fuel performance codes which enables a wide ranging and thorough sensitivity analysis.*

## I. INTRODUCTION

This paper introduces a fuel-cladding gap thermal conductance correlation for mixed oxide fuel elements of sodium cooled fast reactors. The correlation is derived from results obtained using 7 validated fuel performance codes and is expressed as a function of linear heat rating and burn-up. This parameterisation can be used to improve the accuracy and predictive capability of transient analysis of coupled neutronics thermal hydraulics simulations.
The paper first presents the geometry and material characteristics used for the pin model in Section 2. Then, the methodology used to obtain a reliable parametrisation of the gap conductance is detailed in Section 3. Section 4 presents the results for the parametrisation of gap conductance with respect to fuel rating and burnup. In Section 5, the limitations of the parametrisation are discussed and their impact on the uncertainties associated with the gap conductance correlation detailed.

## II. GEOMETRY, MATERIAL SPECIFICATIONS AND REACTOR PHYSICS DATA

### II.A. Geometry

The axial composition of the ESFR-SMART core assemblies for the inner and outer fuel is provided in Figure 1. Cold dimensions (in mm) are provided next to each region, with the axial composition given as subscript.

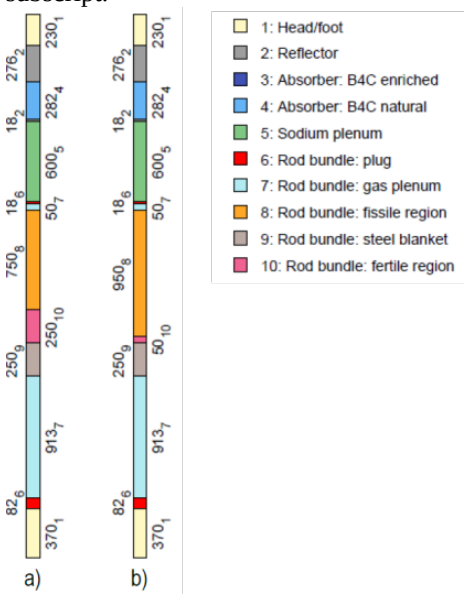


Fig. 1. Axial composition of inner (a) and outer (b) fuel.

The fuel pin geometry for the inner and outer fuel pins is displayed in Table I.

TABLE I. Dimension of fissile and fertile fuel pins

| | Fissile | | Fertile | |
|---|---|---|---|---|
| Dim. in cm | Cold dim. | Nominal dim. | Cold dim. | Nominal dim |
| Pellet inner hole radius | 0.1560 | 0.15816 | NA | NA |
| Pellet radius | 0.4680 | 0.47448 | 0.4680 | 0.47105 |
| Clad inner rad. | 0.4835 | 0.48623 | 0.4835 | 0.48623 |
| Clad outer rad. | 0.5358 | 0.53886 | 0.5358 | 0.53886 |

**II.B. Material specifications**

The fuel in the fissile part is Mixed Oxide fuel (plutonium and uranium oxides) and depleted uranium in the fertile part. Table II details the fresh fuel characteristics.

TABLE II. Fresh fuel characteristics

| | |
|---|---|
| Fissile fuel average density (g.cm$^{-3}$) | 10.542 (95.5% TD) |
| Fertile fuel average density (g.cm$^{-3}$) | 10.457 (95.5% TD) |
| Fresh fuel stoichiometry | 1.97 |
| Fresh fuel porosity (%) | 4.5 |

Even though the cladding material was chosen to be ODS steel in the ESFR-SMART project, the fuel pin models built used austenitic stainless steel commonly referred to as 15-15Ti steel for cladding. The decision was made because the specifications of the ODS steel were not known when the study started. The implications of the change are investigated in the sensitivity study.

**II.C. Reactor physics data**

The study was provided with axial profiles of fuel linear heat rating, neutron flux (above and below 1MeV) and cladding temperatures as a function of burn-up for both inner and outer fuel. These were obtained using through SERPENT [1] neutronics calculations.

**III. METHODOLOGY**

**III.A. Codes and participants**

The following organisations were involved in the study: Wood and the University of Cambridge working with TRAFIC [2]; PSI working with FRED [3]; Framatome and EDF working with GERMINAL [4]; JRC and the University of Cambridge working with TRANSURANUS [5]and KIT working with FEMAXI [6], SIM-SFR [7] and SAS-SFR [8]. In addition, CEA provided technical support to the task.

Because only one fuel performance code is able to model the growth of effects of “Joint Oxyde-Gaine” (JOG) formation [9], a phenomenon occurring for high burn-ups, reference calculations were performed without JOG. The impact of the JOG on gap conductance is discussed in the sensitivity study.

**III.B. Simplified case**

*III.B.1. Simplified model*

The task participants were first asked to produce a simplified model. The aim was to produce and compare preliminary results in order to identify variations between codes, discuss their potential causes and provide solutions.

The simplified case consisted of a fixed axial power profile for both the inner and outer fuel. The axial power profile was taken from the middle-of-life (1200 EFPD) to ensure that a representative power for the axial blanket is utilised.

The cladding temperature provided was used as boundary condition.

Simulations were performed at five power levels, where the total power is adjusted by a scaling factor (equation 1), but the axial power profile and time-dependence of the power remains unchanged. There were therefore 5 simulations per fuel pin type, resulting in 10 simulations altogether.

$$scaling\ factor, f = 0.5;\ 0.75;\ 1.0;\ 1.25;\ 1.5 \quad (1)$$

*III.B.2. Comparison of outputs*

For all 10 simulations, participants were asked to provide the multiple outputs at burn-up steps 1, 300, 600, 900, 1200, 1500, 1800, 2100 EFPDs including gap conductance, gap size, central and surface fuel temperatures.

Results were compared primarily for the 1 EFPD step as it is the simplest condition. This first comparison allowed the identification of mistakes. Subsequent iterations of the simplified model for each code ensured that the results each obtained were in broad agreement.

**III.C. Detailed case**

*III.C.1. Detailed model*

Once the simplified models produced results which were broadly in agreement for the 1 EFPD step, the participants were asked to expand it to include the time-dependent axial power profile. Once again, simulations were performed at various power levels, where the total power is adjusted by a scaling factor, accounting for the time-dependence of both total power and the axial power profile.

*III.C.2. Outputs*

In addition to the outputs already described in Section 3.2.2, task participants were asked to provide the maximum nodal fuel rating and maximum nodal burn-up for each burn-up step in the scaling factor *f* = 1 case. This output was compared with the theoretical values of maximum nodal fuel rating and maximum nodal burn-up computed using the axial power profiles. A close match between the theoretical values and computed ones ensured that no mistake was introduced in the models when the time-dependent axial profile was being included.

### III.D. Parametrisation of the fuel-cladding gap conductance

The aim of the paper is to provide a fuel-cladding gap thermal conductance correlation with two variables, fuel rating (in kW/m) and burn-up (in MWd/tne). The following steps were followed to produce it.
First, the gap conductance at each node each burn-up step for all 10 simulations using the detailed model were compiled from the results provided by each code.
For all these data points, the nodal fuel rating in kW/m was found using the axial power profiles and the nodal burn-up in MWd/tne was computed using equation 2.

$$BU(node = i, burnup\ step = J) = \sum_{j=1}^{J-1} FR(i,j) \times 10^{-3} \times \frac{300\ days}{\rho_{HM} \times A} \quad (2)$$

Where *i* is the node number between 1 and 20, *J* an integral number ranging from 1 to 8, $FR(i,j)$ is the fuel rating at the node number *i* and burnup step *j* in $kW.m^{-1}$, $\rho_{HM}$ the heavy metal density in $tne(HM).m^{-3}$ and $A$ is the axial cross section of the fuel in $m^2$.

This allowed to plot the fuel-cladding gap conductance data points as a function of burn-up and fuel rating. The data points were also segregated between the fertile and fissile regions.

The next step was to find a 2-dimensional function to fit these data points. This was tried for the fertile and fissile data points, as well as for the entire data set.
Multiple fits were tried, including fourth-order polynomials, logarithmic and exponential functions. For each function, the root mean square (RMS) deviation between the data points and the 2-D fit was evaluated. The parameters of the functions were optimised by minimising the RMS.

Finally, a handful of functions with similar RMS were shortlisted and discussed among the authors. Using the expertise and experience of the group, the function that best represented the physical phenomena was picked for the fuel-cladding gap conductance correlation.

## IV. PARAMETERISATION RESULTS

### IV.A. Fuel-Cladding gap conductance correlation

Once the gap conductance data was collected, two-dimensional functions were sought to fit the data. Fits were tried for the data from the fissile and fertile sections separately as well as for the data from the two sections together. In order to optimise the fit, the Root Mean Square of the deviation was calculated and minimised by varying the parameters of the functions tried.
It was found that having a correlation for both the fissile and fertile gap conductance data does not negatively impact the RMS deviation. Thus, Task 1.2.3 proposes a combined correlation for both the fissile and fertile sections of the fuel pin.
The following correlation was chosen to be:

$$h_{gap}(\dot{q}, B) = 10^{-2}(3 + \dot{q}) \times [1 + tanh(2 \times 10^{-5} \times B)] \quad (3)$$

Where $h_{gap}$ is the fuel-cladding gap conductance in $W.cm^{-2}.K^{-1}$, $\dot{q}$ is the linear heat rating in $kW.m^{-1}$ and $B$ is the burn-up in $MWd.t(HM)^{-1}$.
This correlation has the benefits of simplicity whilst capturing the main physical phenomena. Gap conductance increases linearly with the linear heat rating as an increase in local power lead to thermal expansion of the fuel which reduces gap size and to an increase of the gas temperature and conductivity.
In addition, fuel burn-up leads to several competing processes, including:

- Fuel swelling which leads to gap closure and to an increase in gap conductance
- Fission gas release which leads to: (1-) a reduction of the gas mixture thermal conductivity and (2-) to an increase in pressure leading to an increase in cladding diameter by creep; both effects contribute to reduce gap conductance.
- Irradiation swelling of the cladding leading to an increase in gap size and to a reduction in gap conductance.

The impact of fuel swelling on the gap conductance first dominates, but the effects induced by fission gas release and clad irradiation swelling lead to a saturation of heat transfer at high burn-up.

Figure 2 presents the ratio of the correlation gap conductance to the gap conductance calculated by the codes as a function of the gap conductance calculated by codes. It shows a large spread in the results obtained by the different codes. This large spread can be explained by

the fact that the fuel pin behaviour during irradiation involves many competing physical processes, that are strongly coupled and presenting threshold effects for some of them. As a consequence, the predictions of the fuel-to-cladding gap size and composition may largely differ from one code to another at some irradiation times, leading to large discrepancies in the gap thermal conductance evaluation. For all data points, the correlation prediction for gap conductance is between 0.15 and 9.31 times that of the calculated gap conductance, with 95% of the predictions falling between 0.24 and 4.01 times the calculated value.

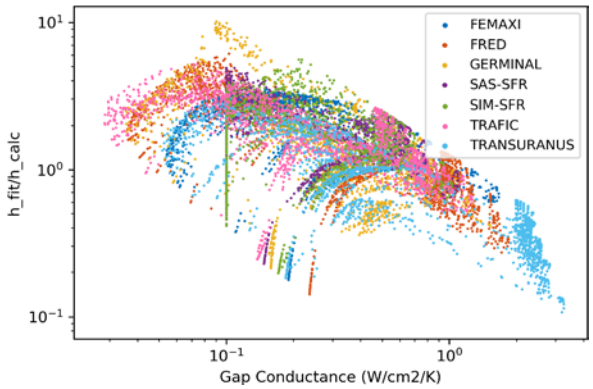


Fig. 2. Ratio of gap conductance of the correlation to gap conductance calculated by codes as a function of gap conductance calculated by codes in logarithmic scale

### IV.B. Axial profile of central fuel temperature

Figure 3 presents the evolution of the axial profile of the central fuel temperature as burn-up increases for the inner fuel and with a power scaling factor of 1, for all codes. It also includes the results obtained by GERMINAL with the gap conductance correlation used (in black).

At 1 EFPD, the central temperature profiles of all codes have all the same shape. The central temperature in the fertile section (from 0 to 25cm) is constant at 700K. The temperature sharply increases at the fission/fertile boundary to 1750K. The axial profile of the central temperature in the fissile region (25cm to 100cm) is bell-shaped, reaching a maximum of 2300K at 62.5cm and finishing at 1850K at the top of the fuel pin. The prediction of GERMINAL using the gap conductance correlation agrees well with the code predictions.

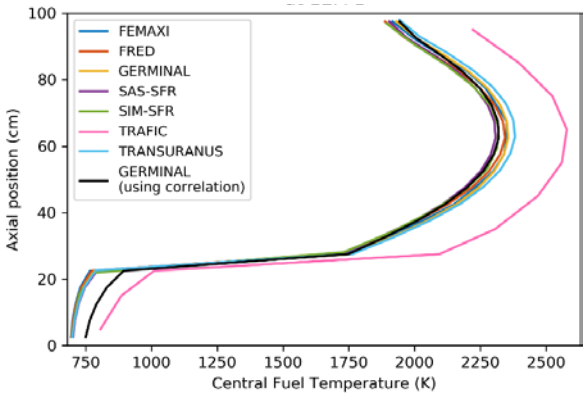


a. Inner fuel, scaling factor = 1, at **1 EFPD**

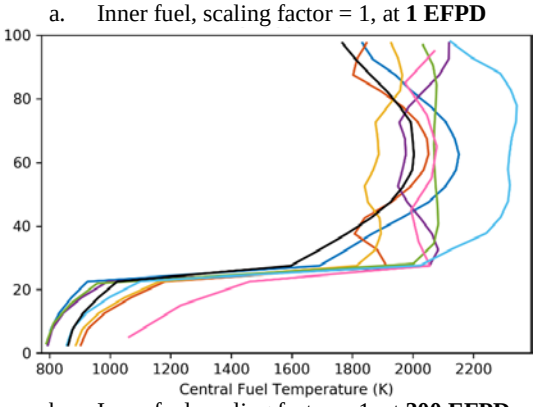


b. Inner fuel, scaling factor = 1, at **300 EFPDs**

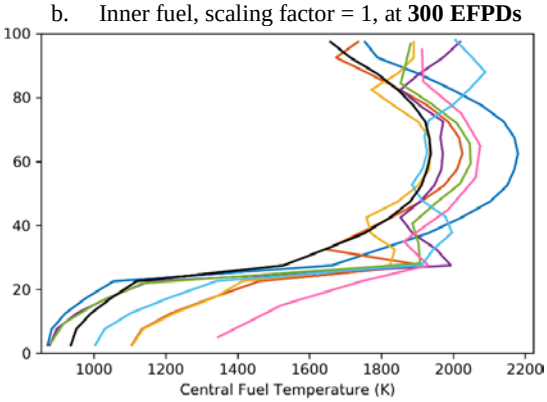


c. Inner fuel, scaling factor = 1, at **600 EFPDs**

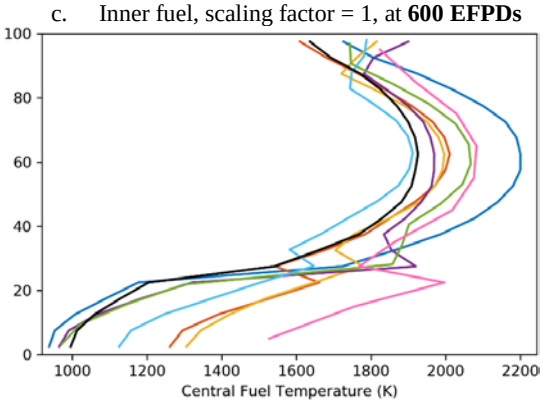


d. Inner fuel, scaling factor = 1, at **900 EFPDs**

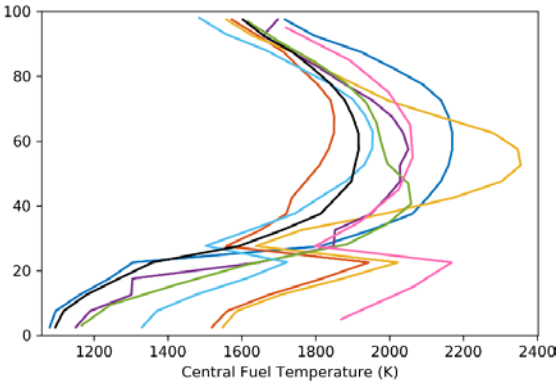


e. Inner fuel, scaling factor = 1, at **1500 EFPDs**

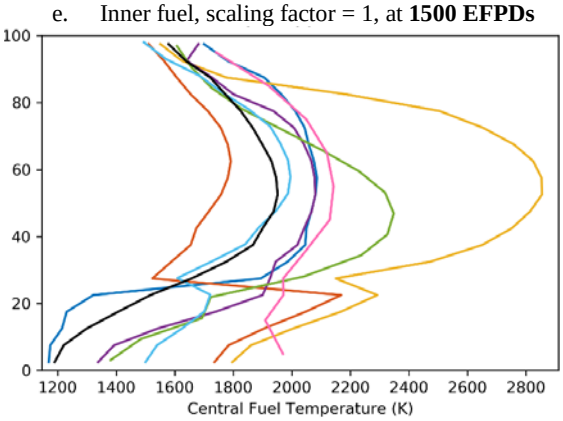


f. Inner fuel, scaling factor = 1, at **2100 EFPDs**

Fig. 3. Axial profile of the central fuel temperature at different burn-up points

At 300 EFPDs, some divergence between code results starts to emerge. However, most codes still provide similar predictions for the central temperature axial profile. The central temperature is lowest at the bottom of the fuel pin. In the fertile region, the temperature slowly increases with the axial position from around 850K at the bottom of the fuel pin to around 1000K at 22.5cm. The central temperature rises sharply at the fissile/fertile region, from around 1000K to around 1850K. In the fissile region, the central temperature is predicted to oscillate with magnitude of 50 to 100K around an average temperature comprised between 1800K and 2000K depending on the code. The prediction for the axial profile of the central temperature using the gap conductance correlation mostly remains in agreement with the predictions of the codes. The predictions for the axial profile are comparable and the prediction made using the correlation for the maximum temperature in the fuel is comprised between the values predicted by the 5 codes. However, it predicts the temperature profile in the fissile region to be a bell-curved, leading to a slight under-prediction of the central temperature at both ends of the fissile region, compared with the other codes' predictions.

Between 600 and 900 EFPDs, the axial profile of the central temperature behaves very similarly than for 300 EFPDs. It is noted however that the differences between codes, in terms of temperature at the bottom and temperature gradient, increases with burn-up. This trend may be explained by increasing differences in the fission gas release predictions. Temperature at the bottom of the fuel pin is comprised between 950K and 1300K at 900 EFPDs. In the fissile region, the axial profile of the temperature slowly reverts to the bell-shaped curve found at 1 EFPD. Both the shape of the central temperature curves and the temperature values predicted by GERMINAL using the gap conductance correlation varies little between 300 EFPDs and 900 EFPDs. As a result, the agreement between the codes' predictions and the prediction made using the gap conductance correlation improves with burn-up.

After 900EFPDs, the divergence between code results becomes significant, in particular in the fertile region and at the fertile/fissile boundary. At the fertile/fissile boundary, the temperature increases sharply, similarly to lower burn-up steps. However, some codes predicts a sharp decrease in temperature of various magnitudes at the next node, while others predict none at all. In the fissile region however, the code predictions for the axial shape of the central temperature are in agreement and have the same bell-shape curve as for lower burn-up steps, with a temperature spread increasing with burn-up. The prediction made using the gap conductance correlation is similar to lower burn-up steps and is slightly under-predicting the temperature in the fertile region. In the fissile region however, the prediction remains in good agreement with the codes' predictions.

At higher burn-ups, the predictions for the central temperature in the fertile region and at the fertile/fissile boundary are very different from code to code and no consensus exists. In the fissile region however, all codes continue to predict a bell-shape curve for the temperature axial profile. The spread of results for the maximum temperature in the fissile section becomes very large however: between 1700K and 2850K at 2100 EFPDs. For the longest times of irradiation, the activation or not of clad swelling represents an additional cause of increasing discrepancies between the codes predictions.

## V. UNCERTAINTY AND SENSITIVITY ANALYSIS

### V.A. Uncertainty analysis

The derived correlation for the gap thermal conductance should be accompanied by recommendations on how to estimate the uncertainty. Since the conducted exercise was totally analytical, without experimental data, one of the approaches to this problem could be based on the analysis of discrepancies between the results obtained with the different codes. The analysis of the reasons of

these discrepancies goes beyond the scope of this paper, because of the complexity of this task determined by the large number of models and material properties involved.

The value of the gap conductance is mainly determined by thermal conductivity of the gas filling the gap, by the gap size and by the fuel-clad contact pressure (in case of a closed gap regime). The evolution of these values during the base irradiation depends on a number of models and material properties (see Figure 4).

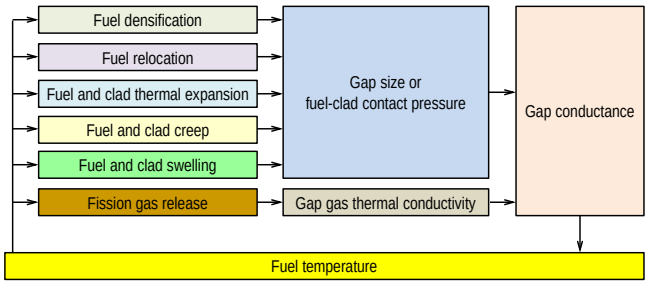


Fig. 4. Some models and material properties which have an impact on gap conductance results

Having in mind the complexity of the detailed comparative analysis of all these models and material properties, we decided to adopt a simple approach to evaluate the uncertainties based on the characterization of the spread of the obtained results. We introduce a multiplier to the proposed correlation and define the Cumulative Distribution Function (CDF) for this multiplier (see Table III) so that for any interval of the multiplier one can find the fraction of the data points (predictions of codes) covered by this interval. For example: if the interval of the gap conductance from $0.33 \times h_{gap}$ to $1.97 \times h_{gap}$ (where $h_{gap}$ is the gap conductance calculated by Eq. 3) contains 80% of the data (predictions of various codes). This approach allows propagation of the methodological uncertainty in Eq. 3 e.g. into the fuel temperature calculations.

TABLE III. Cumulative Distribution Function for multipliers of the gap conductance equation

| **Multiplier** | 0.1 | 0.2 | 0.27 | 0.33 | 0.39 | 0.46 | 0.56 | 0.69 |
|---|---|---|---|---|---|---|---|---|
| **CDF(%)** | 0 | 1 | 5 | 10 | 20 | 30 | 40 | 50 |
| **Multiplier** | 0.85 | 1.02 | 1.3 | 1.97 | 3.03 | 4.99 | 9.31 | |
| **CDF(%)** | 60 | 70 | 80 | 90 | 95 | 99 | 100 | |

### V.B. Sensitivity analysis

The goal of this section is to discuss some results of the sensitivity study in order to provide some advice for the use of the correlation, by assessing the effect of the simplifications necessary to conduct the present study.

#### *V.B.1 Irradiation-induced clad swelling*

The first one is neglect of irradiation-induced clad swelling. A sensitivity analysis has been realized for this study, coming as a consequence of the fact that the constitutive laws for ODS clad material are not available in the public domain. The clad material was thus supposed to be 15-15Ti, steel for which the swelling resistance is very variable when considering different fabrication batches. Comparative calculations have been performed using on one hand the clad mechanical behaviour law as it is, and on the other hand by switching off irradiation-induced swelling. The calculations have been done for inner fuel, for which final damage in cladding is higher than in outer fuel, at normal operating level – scaling factor on power is one. In that case, the maximum damage in cladding is around 160 dpa. The discrepancies between the predictions at the end of irradiation (2100 EFPD) are strongly linked to the activation or not of clad swelling.

The range in the effect of swelling is widespread between codes, from no effective clad swelling when the model is enabled, to intermediate or strong activation of swelling. Without any effective activation of clad swelling, the fuel-to-cladding gap remains closed along the most part of the fissile stack. The estimations of the gap thermal conductance are consequently consistent whether the swelling model is enabled or not, with a maximum around 1 W/cm$^2$/K.

With a strong activation of clad swelling, leading to a gap reopening (the maximum size is around 140 µm), the comparison of the “swelling” and “no swelling” cases shows significant differences. The reopening of a gap only filled with gas – the disabling of JOG formation modelling in the computations represents another limitation, to be discussed further – leads to an important degradation of the heat transfer: the gap thermal conductance is decreasing until 0.1 W/cm$^2$/K for the “swelling” case. This represents one order of magnitude lower when compared to results without effective activation of swelling. The predicted temperature steps in gap differ logically in the same ratio (for the same outgoing heat flux), leading to a significant elevation of maximum temperature in fuel: from 1800°C (no activation of swelling) to 2600°C (strong activation of swelling).

As a conclusion, this sensitivity analysis has shown that the irradiation-induced swelling of clad material can significantly modify the heat transfer when the threshold of clad swelling is exceeded. This effect is comparable to the differences obtained with the various codes in order to obtain the correlation for the gap thermal conductance. The resulting correlation thus relies on the assumption of

a cladding material having a strong resistance to swelling. This assumption is justified for ODS material that has been chosen for the ESFR-SMART fuel pin design, but it also represents a restriction for the use of the correlation.

**The use of the correlation to simulate high performances in terms of burn-up and damage in cladding has to be restricted to clad materials that have effectively demonstrated strong resistance to swelling.**

*V.B.2 "Joint Oxyde Gaine"*

The second important simplification concerns the effect of the "Joint Oxyde-Gaine" formation on the heat transfer in fuel-to-cladding gap. JOG is a compound of released fission products (mainly Cs, Mo, Te) which precipitation in fuel-to-cladding gap has been systematically observed at high burn-up [9] in fuel elements irradiated in PHENIX reactor at normal operating conditions.

When the JOG starts to form, its initial effect on heat transfer is thought to be favourable as it is denser than the gas mixture. JOG should consequently have a better thermal conductivity. But when going further in irradiation, the JOG layer thickness increases progressively with the released quantity of volatile fission products. The consequence is that the ratio of the thermal conductivity divided by the layer thickness is expected to become less favourable; the heat transfer is thus degraded.

Based on the previous "no swelling" case for inner fuel at normal operating level, an additional calculation has therefore been performed with GERMINAL in order to quantify also the effect on the predictions when considering JOG formation modelling. The results led to the following observations:

At the extremities of the fissile stack, the JOG thickness is small and the effect on heat transfer is thus favourable, thanks to a better thermal conductivity. But it is not the same around peak power position: the effect induced by the increase of the JOG thickness becomes preponderant, and the heat transfer is degraded, leading to an elevation of fuel maximum temperature of about 160°C.

For the overall calculations performed to obtain the correlation for the gap thermal conductance, **it was chosen to disregard JOG formation modelling**. This was because it was not available in all fuel performance codes and because it was necessary to preserve as much as possible the consistency of the modelling involved for the calculations performed to obtain the correlation; that is to say, the consistency of the method to obtain the correlation. In addition, the sensitivity analysis that is presented here has brought a quantification of the effect on the results when accounting for JOG formation. The conclusion on that point can thus be drawn in two parts:

- The correlation obtained within this task does not render the effect of JOG formation on heat transfer at high burn-up. This has to be taken into consideration when targeting high performance of fuel element.
- When accounting for JOG formation, the resulting variations in the predictions are comparable to the discrepancies already observed between the different codes applied in the analysis.

## VI. CONCLUSIONS

This paper presents a 2-D correlation for the heat conductance with respect to fuel burn-up and fuel rating based on the results obtained using 7 validated fuel performance codes. In the correlation, the gap conductance is found to increase linearly with the linear heat rating. An hyperbolic tangent was found to best describe the effect of burn-up, as the gap conductance first increases with burn-up before reaching a saturation value. The study also presents fuel performance results obtained using the gap conductance correlation found.
The uncertainty analysis and sensitivity analysis detail the limitations for the use of this correlation. In particular, it should be restricted to clad materials that have demonstrated strong resistance to swelling. In addition, it does not take into account the effect of JOG formation on heat transfer at high burn-up.
.

## ACKNOWLEDGMENTS

The work has been prepared within EU Project ESFR-SMART which has received funding from the EURATOM Research and Training Programme 2014-2018 under the Grant Agreement No. 754501.

## REFERENCES

1. J. Leppänen, M. Pusa, T. Viitanen, V. Valtavirta and T. Kaltiaisenaho, "The Serpent Monte Carlo code: Status, development and applications in 2013.," *Annals of Nuclear Energy,* vol. 82, pp. 142-150, 2015.

2. R. Calabrese, F. Vettraino, C. Artioli, V. Sobolev and R. Thetford, "Heterogeneous fuels for minor actinides transmutation: Fuel performance codes predictions in the EFIT case study," *Annals of Nuclear Energy,* vol. 37, no. 6, pp. 867-874, 2010.

3. K. Mikityuk and A. Shestopalov, "FRED fuel behaviour code: Main models and analysis of Halden

IFA-503.2 tests," *Nuclear Engineering and Design*, vol. 241, pp. 2455-2461, 2011.

4. M. Lainet, B. Michel, J.-C. Dumas, M. Pelletier and I. Ramière, "GERMINAL, a fuel performance code of the PLEIADES platform to simulate the in-pile behaviour of mixed oxide fuel pins for sodium-cooled fast reactors," *Journal of Nuclear Materials,* vol. 516, pp. 30-53, 2019.

5. L. Luzzi, A. Cammi, V. D. Marcello, S. Lorenzi, D. Pizzocri and P. V. Uffelen, "Application of the TRANSURANUS code for the fuel pin design process of the ALFRED reactor," *Nucl. Eng. Des.*, vol. 277 , pp. 173-187, 2014.

6. T. Okawa, I. Tatewaki, T. Ishizu, H. Endo, Y. Tsuboi and H. Saitou, "Fuel behavior analysis code FEMAXI-FBR development and validation for core disruptive accident," *Progress in Nuclear Energy*, vol. 82, pp. 80-85, 2015.

7. G. Bandini, S. Ederli, S. Perez-Martin, M. Haselbauer, W. Pfrang, L. Herranz, C. Berna, V. Matuzas, A. Flores Y Flores, N. Girault and L. Laborde, "ASTEC-Na code: Thermal-hydraulic model validation and benchmarking with other codes," *Annals of Nuclear Energy*, vol. 119, pp. 427-439, 2018.

8. W. M. SCHIKORR, "Assessment of the kinetic and dynamic transient behavior of sub-critical systems (ADS) in comparison to critical reactor systems," *Nuclear Engineering and Design*, vol. 210, pp. 95-123, 2001.

9. M. Tourasse, M. Boidron and B. Pasquet, "Fission product behaviour in Phenix fuel pins at high burnup," *Journal of Nuclear Materials,* vol. 188, pp. 49-57, 1992.